JOURNAL OF VIROLOGY, Feb. 2002, p. 1825–1838 Vol. 76, No. 4
0022-538X/02/$04.00+0 DOI: 10.1128/JVI.76.4.1825–1838.2002

VP40, the Matrix Protein of Marburg Virus, Is Associated with Membranes of the Late Endosomal Compartment

Larissa Kolesnikova, Harald Bugany, Hans-Dieter Klenk, and Stephan Becker*

Institut für Virologie der Philipps-Universität Marburg, D-35037 Marburg, Germany

Received 27 August 2001/Accepted 6 November 2001

Localization of VP40 in Marburg virus (MBGV)-infected cells was studied by using immunofluorescence and immunoelectron microscopic analysis. VP40 was detected in association with nucleocapsid structures, present in viral inclusions and at sites of virus budding. Additionally, VP40 was identified in the foci of virus-induced membrane proliferation and in intracellular membrane clusters which had the appearance of multivesicular bodies (MVBs). VP40-containing MVBs were free of nucleocapsids. When analyzed by immunogold labeling, the concentration of VP40 in MVBs was six times higher than in nucleocapsid structures. Biochemical studies showed that recombinant VP40 represented a peripheral membrane protein that was stably associated with membranes by hydrophobic interaction. Recombinant VP40 was also found in association with membranes of MVBs and in filopodia- or lamellipodia-like protrusions at the cell surface. Antibodies against marker proteins of various cellular compartments showed that VP40-positive membranes contained Lamp-1 and the transferrin receptor, confirming that they belong to the late endosomal compartment. VP40-positive membranes were also associated with actin. Western blot analysis of purified MBGV structural proteins demonstrated trace amounts of actin, Lamp-1, and Rab11 (markers of recycling endosomes), while markers for other cellular compartments were absent. Our data indicate that MBGV VP40 was able to interact with membranes of late endosomes in the course of viral infection. This capability was independent of other MBGV proteins.

The family of *Filoviridae* comprises Marburg virus (MBGV) and Ebola virus (EBOV), which cause a severe and often fatal hemorrhagic disease in human and nonhuman primates. During the reported outbreaks, up to 80% of the cases had a fatal outcome. The recent outbreak of MBGV hemorrhagic fever in the Democratic Republic of the Congo underlines the emerging potential of this pathogen (68). Filoviral infections are pantropic, affecting almost every organ of the infected host. However, the major and primary targets are cells of the mononuclear phagocytic system (55).

The enveloped MBGV particles are composed of seven structural proteins and the nonsegmented negative-strand RNA genome (7, 15). The viral envelope is spiked with homotrimers of the glycoprotein GP (1, 16, 60). Four proteins are components of the nucleocapsid: the nucleoprotein NP (2, 36, 40, 57), the L protein (46), VP35 (45), and VP30 (2). NP, VP35, and L are essential for viral replication and transcription (45); the function of VP30, an NP-binding phosphoprotein, is still unclear (44).

Between the nucleocapsid and the viral envelope, MBGV particles contain two proteins, VP24 and the highly abundant VP40, whose function is not yet elucidated (2, 13). However, the position of VP40 in the genome (third gene), its hydrophobicity, and its abundance within the virions suggest that VP40 represents a homologue of the matrix proteins of other nonsegmented negative-strand RNA viruses.

It is currently believed that matrix proteins orchestrate the budding process of negative-strand RNA viruses since they interact with both other viral proteins (RNP complex) and the plasma membrane (reviewed in references 22 and 38). The detailed mechanisms of these interactions are not well understood. However, it is proposed for the vesicular stomatitis virus M protein that one fraction is transported independently of viral glycoproteins to the plasma membrane, while another fraction of the M protein binds to and thus facilitates the assembly of nucleocapsids. Then, the assembled nucleocapsids bind to regions of the plasma membrane containing the M (and presumably G [3, 10]) proteins. For Sendai virus it is on the one hand suggested that transport of M proteins to the site of budding might occur along the secretory pathway in association with membrane vesicles containing the viral glycoproteins (59). On the other hand, it is proposed that Sendai virus M protein is recruited at the internal cytoplasmic membranes by the nucleocapsids and then transported to the plasma membrane, where the interaction with the surface proteins takes place (65). Localization of filoviral matrix proteins and, hence, the potential sites of their interactions with viral and cellular structures are still unclear.

Immunoelectron microscopic analysis of MBGV-infected cells detected VP40 inside viral inclusions, indicating that VP40 is somehow associated with the nucleocapsids (23). However, it is unclear whether VP40 is located exclusively in viral inclusions and whether it is transported to the sites of budding together with the nucleocapsids or independently.

The structure of VP40 of EBOV has been elucidated by X-ray crystallography. These studies show that VP40 is a membrane-binding protein, which forms oligomers upon contact with lipid membranes (54, 62). It was further demonstrated that EBOV VP40 can mediate its own release from transfected cells, a function that relies on the integrity of a WW-binding domain at the N terminus (29, 33). These data point out that

* Corresponding author. Mailing address: Institut für Virologie der Philipps-Universität Marburg, Robert-Koch-Strasse 17, D-35037 Marburg, Germany. Phone: 49-6421-2865433 Fax: 49-6421-2865482. E-mail: becker@mailer.uni-marburg.de.

EBOV VP40 might be transported to the plasma membrane independently of other viral proteins and might play an important role during viral budding. The membrane-binding capability and functional characteristics of MBGV VP40 are unknown.

We studied here the localization of VP40 in MBGV-infected cells. VP40 was identified in viral inclusions, associated with individual nucleocapsids, and in the foci of viral budding. Additionally, VP40 was detected in clusters of intracellular membranes and in plasma membrane protrusions. When the localization of recombinant VP40 was investigated, it was found to be firmly associated with membrane structures that have several characteristics of late endosomal compartment. Our data indicate that MBGV VP40 is able to interact with membranes of the late endosomal compartment independently of other viral proteins.

MATERIALS AND METHODS

Viruses and cell lines. The Musoke strain of MBGV, isolated in 1980 in Kenya (64), was propagated in C1008 cells and purified as described previously (20). MVA-T7 was grown and titers were determined in chicken embryo fibroblasts (60). C1008 cells, a cloned cell line of Vero cells (ATCC CRL 1586), Vero cells, and HeLa cells were cultured in Dulbecco modified Eagle medium (DMEM) containing 10% fetal calf serum. For all transfections, HeLa cells were grown in six-well plates (7 cm^2) in DMEM containing 10% fetal calf serum. Monocytes/macrophages were isolated and cultivated as described previously (14).

Antibodies. For the identification of MBGV VP40, a mouse monoclonal antibody (kindly provided by the Centers for Disease Control, Atlanta, Ga.) and a rabbit affinity-purified serum against VP40 were used. For the identification of annexin II, BiP/GRP78, early endosome antigen 1 (EEA1), lysosome-associated membrane protein-1 (Lamp-1), GM130, integrin alpha 2 (VLA-2α), and Rab11, we used monoclonal antibodies from Transduction Laboratories (BD, Heidelberg, Germany). Mouse monoclonal antibody against α-tubulin and a rabbit immunoglobulin G (IgG) against actin were obtained from Sigma (Deisenhofen, Germany). For the identification of filamentous actin, we used phalloidin conjugated with fluorescein isothiocyanate (FITC; Sigma). Respective secondary antibodies conjugated with FITC or rhodamine (for immunofluorescence), with horseradish peroxidase for Western blot, or with colloidal gold (for immunoelectron microscopy) were from Dianova (Hamburg, Germany) or from Dako (A/S, Copenhagen, Denmark).

Detergent treatment of virions and immunoelectron microscopic analysis. Purified virions were fixed with 0.5% paraformaldehyde for 15 min at 4°C and then treated with with 0.05% Triton X-100 for 15 min at 4°C. Detergent-treated and untreated control samples were fixed with 4% paraformaldehyde for 15 min and purified by centrifugation through a 20% sucrose cushion in a Beckman SW41 rotor at 27,000 rpm for 90 min. Pellets were resuspended in TNE (10 mM Tris-HCl, pH 7.4; 0.15 M NaCl; 2 mM EDTA) containing 4% paraformaldehyde. A drop of the virus suspension was deposited on a Formvar-carbon-coated nickel grid for 1 min, the excess fluid was blotted away with Whatman filter paper, and the grids were floated on a drop of phosphate-buffered saline (PBS) containing 1% bovine serum albumin for 10 min. Indirect immunostaining was performed by incubation with an anti-VP40 monoclonal antibody for 60 min, and bound antibodies were detected with a donkey anti-mouse IgG antibody coupled to 6-nm gold particles (Dianova). After being washed with PBS, the samples were negatively stained with 2% phosphotungstic acid and examined in a Zeiss 109 electron microscope.

Subcellular fractionation and membrane association assay. Subconfluent HeLa cells (5×10^5 cells in 7 cm^2 wells) were infected at a multiplicity of infection of 3 to 5 PFU of MVA-T7 per cell. At 1 h postinfection (p.i.), cells were transfected with 1 μg of pTM-VP40, containing the entire open reading frame of the VP40 gene under the control of the T7-RNA polymerase promoter, by using the Lipofectin precipitation method (17).

At 16 h posttransfection, cells were washed three times with lysis buffer (10 mM Tris, pH 7.5; 0.25 M sucrose; 1 mM EDTA; 200 μM orthovanadate; 1 mM phenylmethylsulfonyl fluoride) at 4°C, scraped off the dish in a minimal volume of lysis buffer, and lysed by 10 strokes through a 20-gauge needle. Nuclei were pelleted for 5 min at 800 × *g* for 5 min at 4°C. Sucrose was added to the postnuclear supernatant to a final concentration of 63%. The sample was placed at the bottom of a centrifuge tube and overlaid with 45 and 10% sucrose. The step gradient was then centrifuged to equilibrium at 35,000 rpm overnight. Fractions were collected from the top. Equal amounts of each fraction were analyzed by sodium dodecyl sulfate-polyacrylamide gel electrophoresis (SDS-PAGE) and Western blotting.

Western blotting. Western blot analysis was carried out as described previously (1). The used antibodies and the respective dilutions are given in the figure legends.

Triton X-114 phase-partitioning analysis. The phase-partitioning analysis was done according to the method of Bordier (4). VP40 was expressed in HeLa cells by using the vaccinia virus-T7 expression system. At 16 h posttransfection, cells were scraped into ice-cold lysis buffer, disrupted with 10 strokes through a 20-gauge needle, and subjected to centrifugation for 5 min at 800 × *g* and 4°C to remove nuclei and cell debris. The postnuclear supernatant was mixed with Triton X-114 (final concentration, 1% Triton X-114) in an ice-water bath until the solution was clear. The sample was centrifuged at 14,000 × *g* for 15 min at 4°C. The pellet (insoluble fraction) was recovered with sample buffer. The supernatant was laid over a sucrose cushion (6% [wt/vol] sucrose; 10 mM Tris, pH 7.8; 150 mM NaCl; 0.06% Triton X-114), warmed for 3 min at 30°C, and then centrifuged at 500 × *g* for 3 min at room temperature. The detergent (lower) and aqueous (upper) phases were recovered separately and analyzed by Western blotting.

Indirect immunofluorescence microscopy and immunoelectron microscopy. Cells were fixed with 4% paraformaldehyde and proceeded for immunofluorescence analysis as previously described (2). Immunoelectron microscopy was performed according the method of Kolesnikova et al. (36). Briefly, cells were fixed with 4% paraformaldehyde, dehydrated, and embedded in LR Gold. Indirect immunogold labeling was carried out with ultrathin sections. The used antibodies and their respective dilutions are given in the figure legends. For the quantification of gold particles in the VP40-positive structures, 20 micrographs were taken at a primary magnification of ×50,000. The density of gold labeling at the surface of profiles of VP40-positive structures was determined by morphometric methods (69). Micrographs were scanned by using the Leafscan 45, and the surface of profiles of VP40-positive structures was measured by using the Raytest TINA software.

RESULTS

VP40 is located in viral inclusions and in tubular-vesicular structures. To study the subcellular localization of VP40 by immunofluorescence analysis, human macrophages were infected with MBGV, fixed at 2 days p.i., and immunostained by using a monoclonal antibody against VP40 and a guinea pig antibody against NP. Figure 1A, D, G, and J show that VP40 is associated with different intracellular structures. VP40 was colocalized with NP in the viral inclusions (Fig. 1A to L, arrowheads), which contain preformed nucleocapsids in different states of maturation as shown previously (36). VP40 appeared also in tubular and vesicular structures of various size, which did not contain NP (Fig. 1A, D, and G, arrows). The tubular and vesicular structures were either located in the perinuclear area or close to the plasma membrane (Fig. 1A and D, arrows), and sometimes VP40 was concentrated in bright spots (Fig. 1G, arrow). The majority of VP40-expressing cells displayed both VP40-positive structures (60%). However, in a minor part of the cells VP40 was found predominantly in the viral inclusions (40%, Fig. 1J and L).

The VP40-positive tubular-vesicular structures represent clusters of intracellular membranes. To further investigate the localization of VP40 in MBGV-infected cells, an immunoelectron microscopic analysis was performed. MBGV-infected human macrophages were fixed at 2 days p.i., dehydrated, and embedded in acrylic resin (LR Gold). Indirect immunogold double labeling was carried out with ultrathin sections to detect VP40 (6-nm gold particles) and NP (12-nm gold particles; Fig. 2).

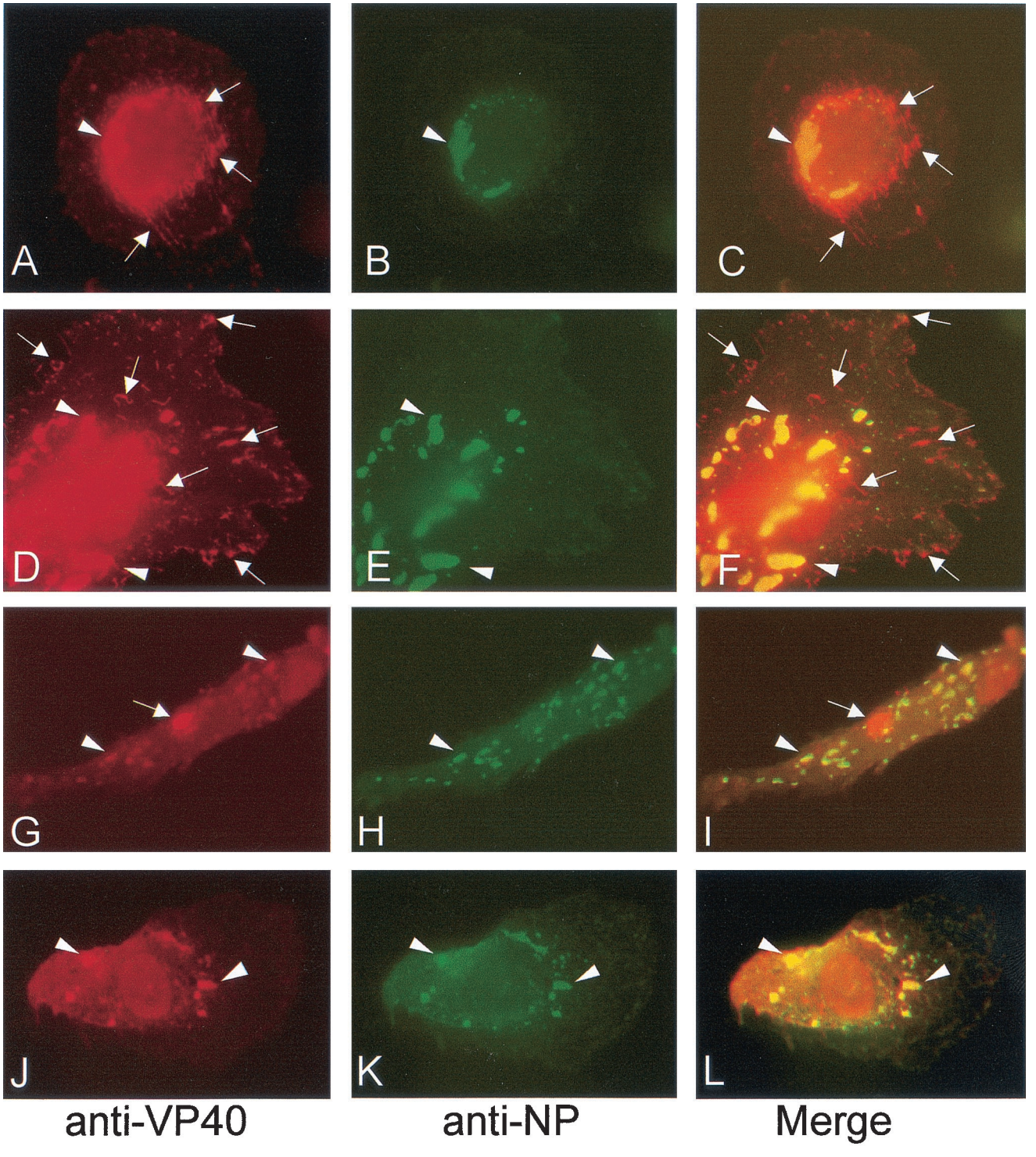

FIG. 1. Indirect immunofluorescence analysis of VP40 and NP distribution in MBGV-infected human macrophages. Human macrophages were infected with MBGV and fixed at 48 h p.i. Immunofluorescence analysis was performed with an anti-VP40 monoclonal antibody (dilution, 1:100) and a secondary donkey anti-mouse antibody conjugated with rhodamine (dilution, 1:100), together with a guinea pig anti-NP serum (dilution, 1:100) and a secondary donkey anti-guinea pig antibody conjugated with FITC (dilution, 1:100). (A, D, G, and J) Anti-VP40/rhodamine. (B, E, H, and K) Anti-NP/FITC. (C, F, I, and L) Merged images. The arrowheads indicate colocalization of VP40 and NP. The arrows indicate singly located VP40.

We found VP40 and NP colocalized at sites of viral budding and inside the released virions (Fig. 2A, arrows point to gold particles indicating VP40). Colocalization of VP40 and NP was also detected in nucleocapsids located outside the viral inclusions (Fig. 2A, inset; the arrow points to VP40 [6-nm gold particle]) and, consistent with the immunofluorescence analysis, in the electron-dense viral inclusions (Fig. 2B, arrows point to VP40 inside the inclusion).

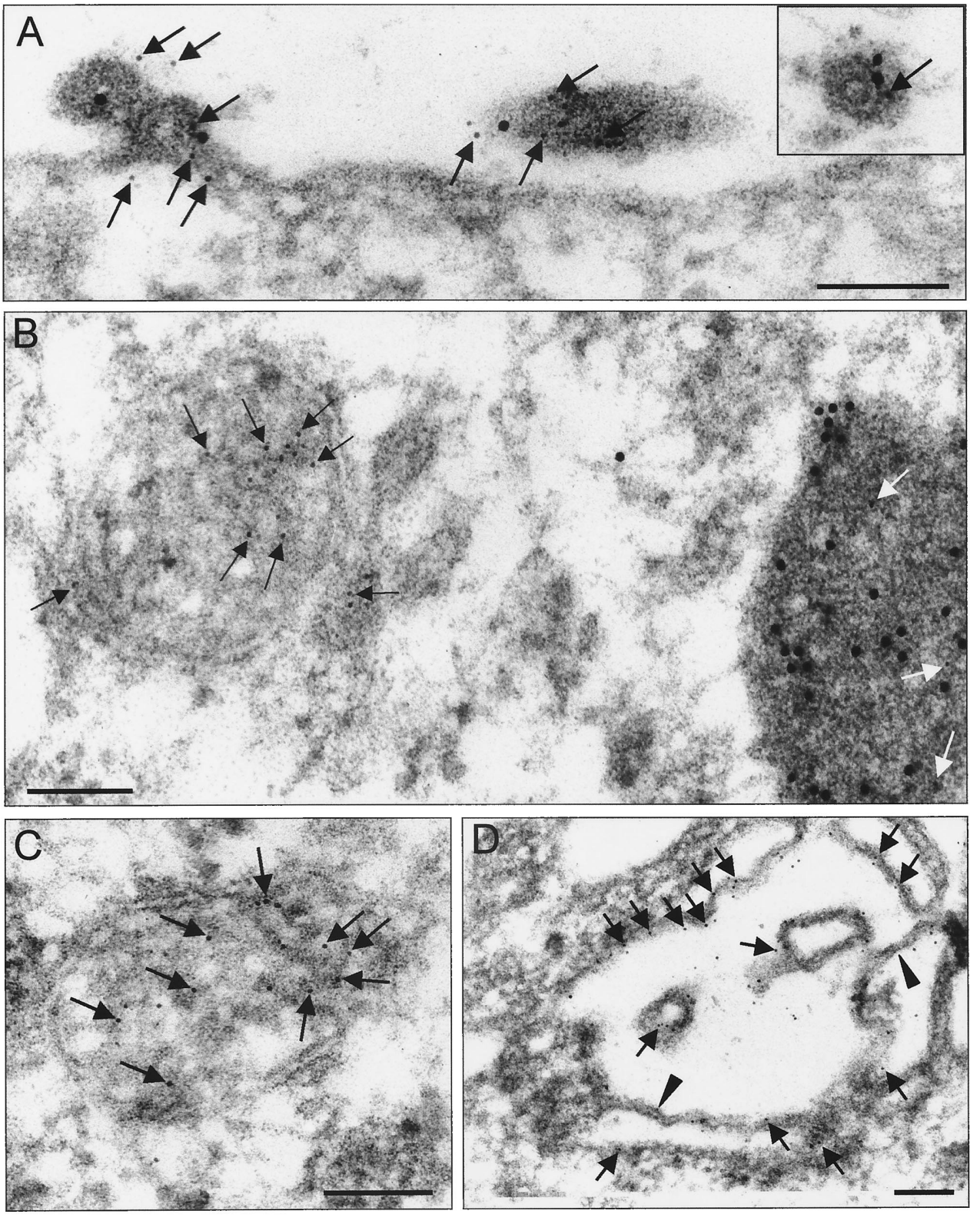

FIG. 2. Immunoelectron microscopic analysis of VP40 and NP distribution in MBGV-infected human macrophages. Human macrophages were infected with MBGV and fixed at 48 h p.i. (A to D) Immunoelectron microscopic analysis was performed with an anti-VP40 monoclonal antibody (dilution, 1:100) and a secondary donkey anti-mouse antibody conjugated with colloidal gold (bead diameter, 6 nm; dilution, 1:25), together with a guinea pig anti-NP serum (dilution, 1:100) and a secondary donkey anti-guinea pig antibody conjugated with colloidal gold (bead diameter, 12 nm; dilution, 1:25). The black and white arrows indicate VP40 (6-nm gold beads). The arrowheads indicate sites of VP40-positive double membranes. Bar, 100 nm. (A) Focus of viral budding. (B) Multivesicular body in direct vicinity of a viral inclusion. (C) Multivesicular body in cytoplasm. (D) Unfolded multivesicular body beneath plasma membrane. (E) Transmission electron microscopy. The arrow indicates viral particles. The arrowheads indicate sites of double membranes. Vi, viral inclusion. Bar, 1,000 nm. (F) Presence of VP40 in protrusions (12-nm gold beads). Bar, 100 nm. (G) NP inside the protrusions is restricted to virions (6-nm gold bead). Bar, 100 nm.

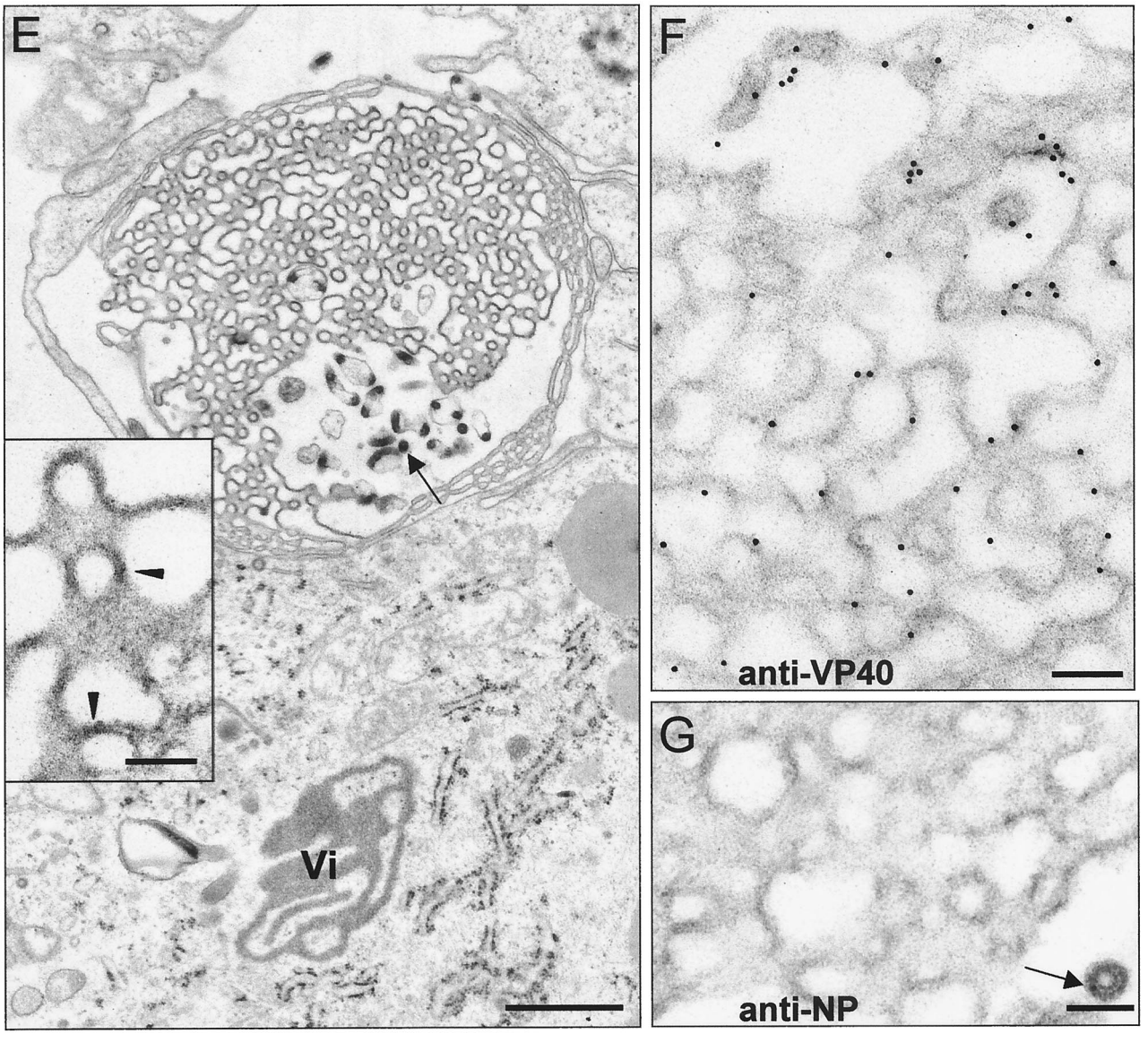

FIG. 2—*Continued.*

Additionally, VP40 was detected in clusters of intracellular membranes (Fig. 2B, left side). In these clusters, neither profiles of nucleocapsids nor NP labeling were detected. The membrane clusters had the appearance of circular vesicles with a diameter of 250 to 1,000 nm. They displayed a multilayered or multivesicular interior (Fig. 2C) reminiscent of endocytic carrier vesicles or multivesicular bodies (MVBs) (25, 34, 67). VP40 was predominantly detected in association with internal membranes of the clusters (Fig. 2B and C, black arrows). VP40-positive membrane clusters were found both in the perinuclear region of the cell and close to the plasmalemma. Often, VP40-positive membrane clusters were located not far from viral inclusions (Fig. 2B). Unfolded profiles of heavily gold-labeled multilayered membrane clusters were detected beneath the plasmalemma (Fig. 2D, arrows point to VP40) and in the foci of plasma membrane proliferation at sites where virus budding could also be detected (Fig. 2E, arrows point to virions, and Fig. 2F). These foci of intense membrane proliferation were characterized by curved sheets of membranes which at some sites made close contacts forming double membranes (Fig. 2E, inset, arrowheads). Figure 2F and G show that VP40-positive protrusions were free of NP except for sites where simultaneously nucleocapsids were detected (Fig. 2G, arrow). A diffusive accumulation of VP40 beneath the plasma membrane outside the foci of budding was not observed.

To analyze the ratio of membrane-bound and inclusion-associated VP40, a morphometric analysis was carried out on ultrathin sections of MBGV-infected cells (26, 69). The density of gold particles (particles per square micrometer of profile of the evaluated structure), representing monoclonal antibodies bound to VP40 molecules, was determined in the profiles of viral particles and intracellular virus-induced structures. Among the latter, we differentiated (i) intracellular VP40-positive membrane clusters, (ii) foci of plasma membrane pro-

liferation, and (iii) viral inclusions and individual nucleocapsids. The number of gold particles in viral inclusions was 40 ± 6 per μm^2, while in membrane clusters and foci of proliferation the densities of gold labeling were 254.8 ± 23 and 259.2 ± 21 per μm^2, respectively. The highest density of gold particles (285.9 ± 20 per μm^2) was found in released viral particles, which approximately equaled the sum of gold density associated with viral inclusions and membranes.

Recombinant VP40 is associated with intracellular membranes. To address the question whether VP40 is able to interact with membranes in the absence of other viral proteins, VP40 was recombinantly expressed from cDNA. HeLa cells were infected with a recombinant vaccinia virus that expresses the T7 RNA polymerase (MVA-T7) and then transfected with the plasmid pTM-VP40, encoding VP40 under the control of the T7 promoter. The cells were fixed at 16 h posttransfection and subjected to immunofluorescence analysis. VP40 was distributed as a cytoplasmic tubular-vesicular network which was concentrated in the nuclear region (Fig. 3A and B) or located closer to the plasma membrane (Fig. 3C and D). Confocal microscopy revealed that VP40 was predominantly located perinuclearly, although a weak intranuclear signal was observed (Fig. 3E). Additionally, VP40 was concentrated beneath the plasma membrane at the leading edges of the cells (Fig. 3A, C, and D, arrows). Finally, VP40 was found to be located in bright spots that were very similar to the VP40-positive spots found in MBGV-infected cells (Fig. 3B and C, arrowheads). Costaining with phalloidin-FITC showed that VP40-positive structures colocalized with actin filaments (Fig. 3E to G).

To analyze whether VP40 was associated with cellular membranes in the absence of other viral proteins, a flotation analysis was carried out. This method identifies integral membrane and membrane-associated proteins by their ability to float together with membrane vesicles in a discontinuous sucrose gradient, while soluble proteins remain at the bottom of the gradient (3). HeLa cells, expressing VP40, were lysed at 6, 12, and 16 h posttransfection, and the lysate was placed at the bottom of a sucrose gradient and subjected to gradient centrifugation. Fractions were collected from the top and analyzed by SDS-PAGE and Western blotting (Fig. 4A). Under these conditions, at all tested time points, the majority of VP40 was found at the 45-to-10% sucrose interface (fractions 3 and 4), while a small amount was detected in the loading zone (fraction 11). These data indicate that VP40 is, indeed, predominantly associated with cellular membranes.

To investigate the nature of the VP40-membrane interaction, we carried out a Triton X-114 phase-partitioning analysis, which differentiates between integral and peripheral membrane proteins. The postnuclear supernatant of VP40-expressing HeLa cells was incubated with Triton X-114 and centrifuged to separate the aqueous (peripheral membrane proteins) and detergent (integral membrane proteins) phases. Figure 4B shows the results of this analysis for VP40, and Lamp-1, an integral membrane protein. While Lamp-1 was found predominantly (95%) in the detergent phase of the extraction, the majority of VP40 (95%) was found in the aqueous phase, indicating that VP40 represents a peripheral membrane protein.

The interaction between VP40 and cellular membranes was further analyzed by treating postnuclear supernatants of VP40-expressing HeLa cells with either high salt concentrations, EDTA, or high pH. Then, samples were subjected to flotation analysis. It can be seen in Fig. 4C that all of these incubation conditions did not induce the detachment of VP40 from the membranes. These findings demonstrated that VP40 (i) is bound to the membranes via hydrophobic interactions (resistance against high salt), (ii) the interaction is not dependent on the presence of divalent cations (resistance against EDTA), and (iii) VP40 is not a soluble luminal protein (resistance against pH 11 [18]).

It was then of interest to characterize the membranes that are able to bind VP40. Thus, Western blots of the fractions gained by flotation analysis were probed with antibodies against several marker proteins of cellular compartments (Fig. 4D). We detected marker proteins of plasma membrane (VLA-2α), endoplasmic reticulum (BiP/GRP78) and late endosomes (lysosome-associated membrane protein-1) in the same fractions as VP40. Annexin II, an abundant protein which is present in the cytosol and on the cytoplasmic face of plasma membrane and early endosomes (28), was found predominantly in the loading zone, while a small portion that was associated with membranes was also detected in fractions 3 and 4.

VP40-positive membranes are associated with Lamp-1 and TfR. The performed flotation analysis did not allow to identify the intracellular membrane compartments which bound VP40 since all cellular membranes migrated in the sucrose gradient with approximately the same velocity. Therefore, we carried out immunofluorescence analyses with VP40-expressing HeLa cells. Cells were simultaneously incubated with an anti-VP40 antibody, together with antibodies against markers of various cellular compartments. We found that the VP40-positive membranes contained Lamp-1, and the transferrin receptor (TfR) (Fig. 5). The anti-VP40 and anti-Lamp-1 staining localized to the same region of transfected cells, but only a partial overlap of the two proteins was observed in the tubular-vesicular network and in spots (Fig. 5A to F, arrows). Double labeling with anti-VP40 and anti-TfR showed colocalization at the leading edge of the cell (Fig. 5G to I) and in spots (Fig. 5J to L, thick arrows). In both cases, colocalization was not complete, and some of the Lamp-1- or TfR-positive membrane clusters were VP40-negative and vice versa (e.g., Fig. 5K and L, arrowheads). VP40-positive membranes did not contain marker proteins of the endoplasmic reticulum, Golgi, and early endosomes (not shown).

We then performed immunoelectron microscopic analyses of HeLa cells expressing VP40. VP40 was found to be associated with membrane clusters of the same multivesicular or multilayered structure as in MBGV-infected cells. The clusters contained Lamp-1 (Fig. 6A and B, arrows), and sometimes TfR (data not shown). Thus, VP40-positive structures are presumed to represent MVBs which functionally belong to the late endosomal compartment (25, 34, 67). VP40-positive membranes were found in the perinuclear region (Fig. 6A), in the cytoplasm (Fig. 6 B), close to the plasmalemma (not shown), and in form of filopodia- or lamellipodia-like protrusions at the surface of the cell (Fig. 6C and D). Lamellipodia-like protrusions were formed by curved sheets of membrane which at some sites contacted closely, forming double membranes (Fig. 6D, arrowhead). Foci of VP40-positive protrusions at the sur-

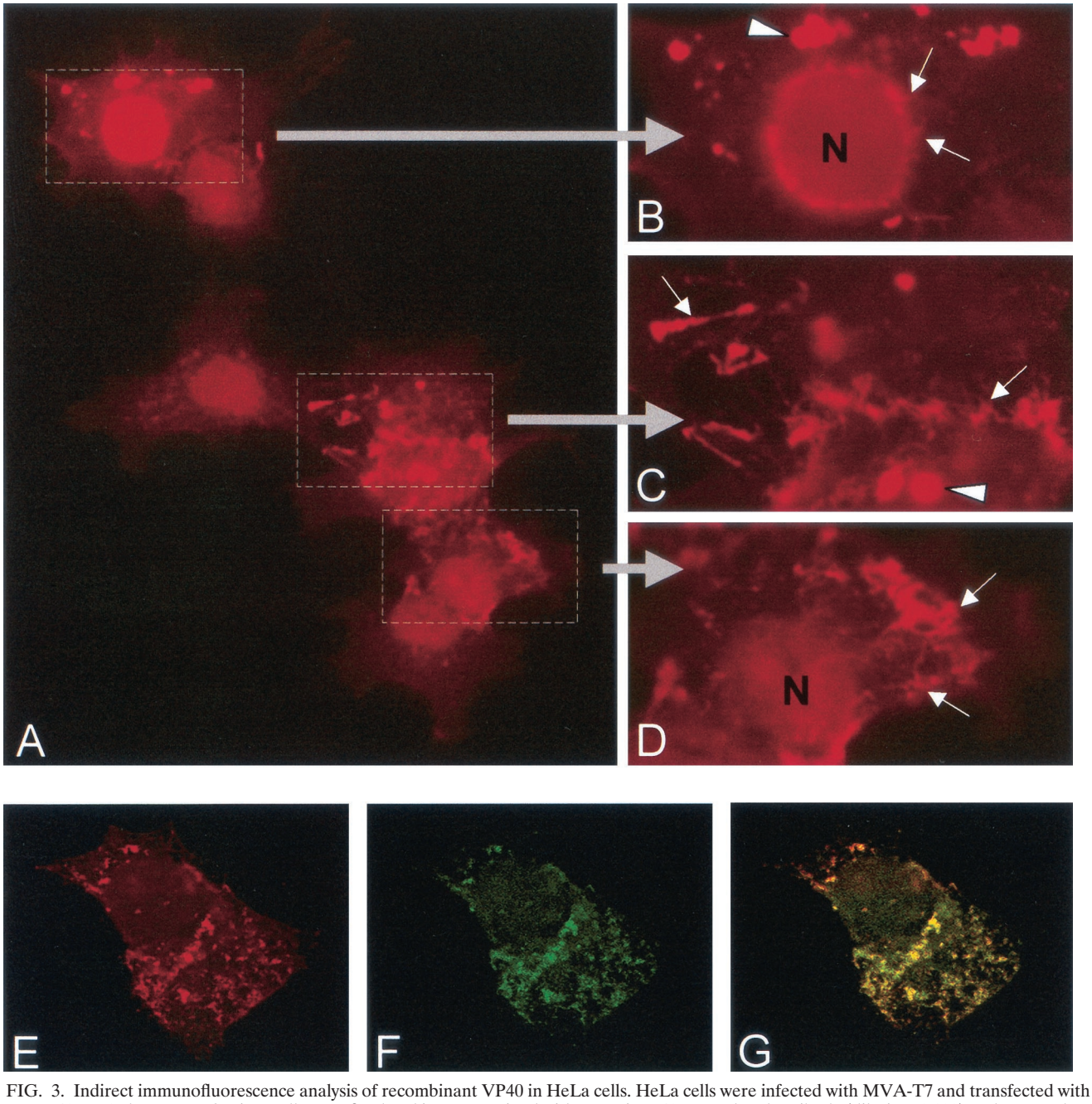

FIG. 3. Indirect immunofluorescence analysis of recombinant VP40 in HeLa cells. HeLa cells were infected with MVA-T7 and transfected with pTM-VP40. At 16 h posttransfection, cells were fixed and immunostained with an anti-VP40 monoclonal antibody (dilution, 1:100) and a secondary donkey anti-mouse IgG conjugated with rhodamine (dilution, 1:100). (A) Distribution of recombinant VP40. The framed parts are shown at a higher magnification in panels B to D. The arrows indicate the tubular network; the arrowheads indicate bright spots. (E to G) Colocalization of actin and VP40 (confocal micrograph). (E) Distribution of VP40. (F) Distribution of filamentous actin. (G) Merge of panels E and F.

face of the cells confirmed that VP40 can be transported to the plasma membrane independently of other viral proteins.

For the formation of its lipid envelope, MBGV needs to recruit cellular membranes. It is considered that the envelope is derived from the cellular plasma membrane; however, the plasma membrane itself has different sources, including endosomes or components of the Golgi apparatus (12). Observations that VP40 was able to associate with membranes of late endosomes suggested that this cellular compartment might be a potential source for the viral envelope. The formation of viral membrane is thought to involve a process of stringent protein sorting with the result that cellular proteins are displaced by viral envelope proteins (reviewed in reference 22). However, since it has been shown that during the budding of rhabdoviruses traces of cellular membrane proteins are incorporated into the viral envelope (39), it was of interest to determine whether cellular proteins were also incorporated into the MBGV envelope, which might point to the cellular origin of

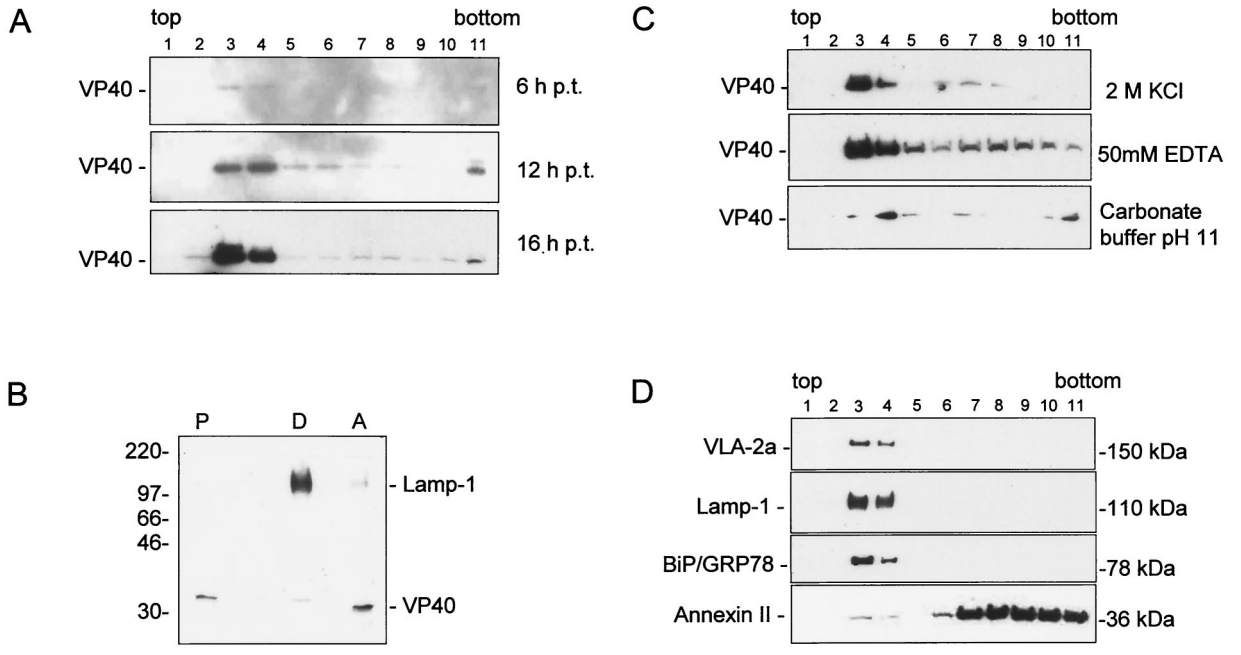

FIG. 4. Membrane association of VP40. (A) HeLa cells were infected with MVA-T7 and transfected with pTM-40. The cells were harvested and lysed at 6, 12, and 16 h posttransfection. Sucrose was added to the postnuclear supernatant to a final concentration of 63%. The sample was placed at the bottom of centrifuge tube and overlaid with 45 and 10% sucrose. The gradient was centrifuged to equilibrium at 35,000 rpm overnight in an SW41 rotor. Fractions were collected from the top, and samples were separated by SDS-PAGE and blotted onto polyvinylidene difluoride membranes. Membranes were stained with an anti-VP40 monoclonal antibody (dilution, 1:1,000). Top of the gradient, fraction 1; bottom of the gradient, fraction 11. (B) Triton X-114 phase-partitioning analysis of VP40 at 16 h posttransfection. HeLa cells were infected and transfected as described for panel A. The postnuclear supernatant was partitioned into aqueous (lane A), detergent (lane D), and insoluble (lane P) fractions as described in Materials and Methods. Staining was done with an anti-LAMP-1 monoclonal antibody (dilution, 1:250) and with an anti-VP40 monoclonal antibody (dilution, 1:1,000). (C) Characterization of the membrane association of VP40 at 16 h posttransfection. Flotation analysis of postnuclear supernatant of recombinant VP40 was carried out as described for panel A. The postnuclear supernatant was treated before flotation analysis with either 2 M KCl (upper panel), EDTA (middle panel), or high pH (lower panel). Western blots were stained with an anti-VP40 monoclonal antibody (dilution, 1:1,000). (D) Characterization of cellular proteins comigrating with VP40 in flotation analysis. Western blots were stained with monoclonal antibodies directed against marker proteins of plasma membrane (VLA-2α), late endosomes (Lamp-1), endoplasmic reticulum (BiP/GRP78), and annexin II.

the viral membrane. Gradient-purified MBGV structural proteins were Coomassie blue stained (Fig. 7A) and in parallel blotted and incubated with antibodies against cellular proteins. The Coomassie blue-stained gel did not reveal considerable amounts of cellular proteins incorporated into the virions (Fig. 7A). The Western blot, however, showed that the preparation contained traces of Lamp-1, Rab11 (marker for recycling endosomes), and actin (Fig. 7B). Marker proteins of the plasma membrane (VLA-2α), endoplasmic reticulum (BiP/GRP78), microtubules (α-tubulin), and early endosomes (EEA1), and one of the most abundant cellular proteins, annexin II, were absent (28). The presence of Lamp-1 and Rab11 in the virions point to the fact that the process of MBGV assembly is at some stages closely associated with the compartment of late endosomes.

VP40 is closely attached to the lipid membrane of the virion. To determine the localization of VP40 inside the virion, the supernatant of MBGV-infected Vero cells was harvested and concentrated at 5 days p.i. The virus suspension was prefixed with 0.5% paraformaldehyde and then treated with 0.05% Triton X-100 to remove the lipid envelope. Virions were purified by centrifugation and prepared for immunoelectron microscopy. Samples were incubated with a monoclonal antibody directed against VP40, followed by a secondary antibody conjugated to colloidal gold. As shown in Fig. 8A, treatment of the virions with Triton X-100 removed the viral envelope and resulted in partially naked nucleocapsid structures. Aggregates, which were formed by the removed viral envelope, could also be detected (Fig. 8B). Weak gold labeling was observed in areas of the nucleocapsid coil, where the nucleocapsid-surrounding matrix was not completely stripped off (Fig. 8A, arrows). VP40 was also detected, and in larger amounts, in the aggregates that were formed by the removed viral envelope (Fig. 8B). These results demonstrated that MBGV VP40 was closely associated with the lipid bilayer. Virions, which were not treated with detergent, did not show labeling of the outer surface, suggesting that VP40 does not protrude through the virus membrane (Fig. 8C). Our data show that the removal of the viral membrane resulted in the simultaneous removal of the majority of VP40, which appeared to be closely associated with the inner side of the envelope. Thus, the intravirion localization of VP40 is similar to that of M proteins of other *Mononegavirales* which form a dense layer, tightly associated with the inner leaflet of the lipid bilayer (6, 19, 48, 50).

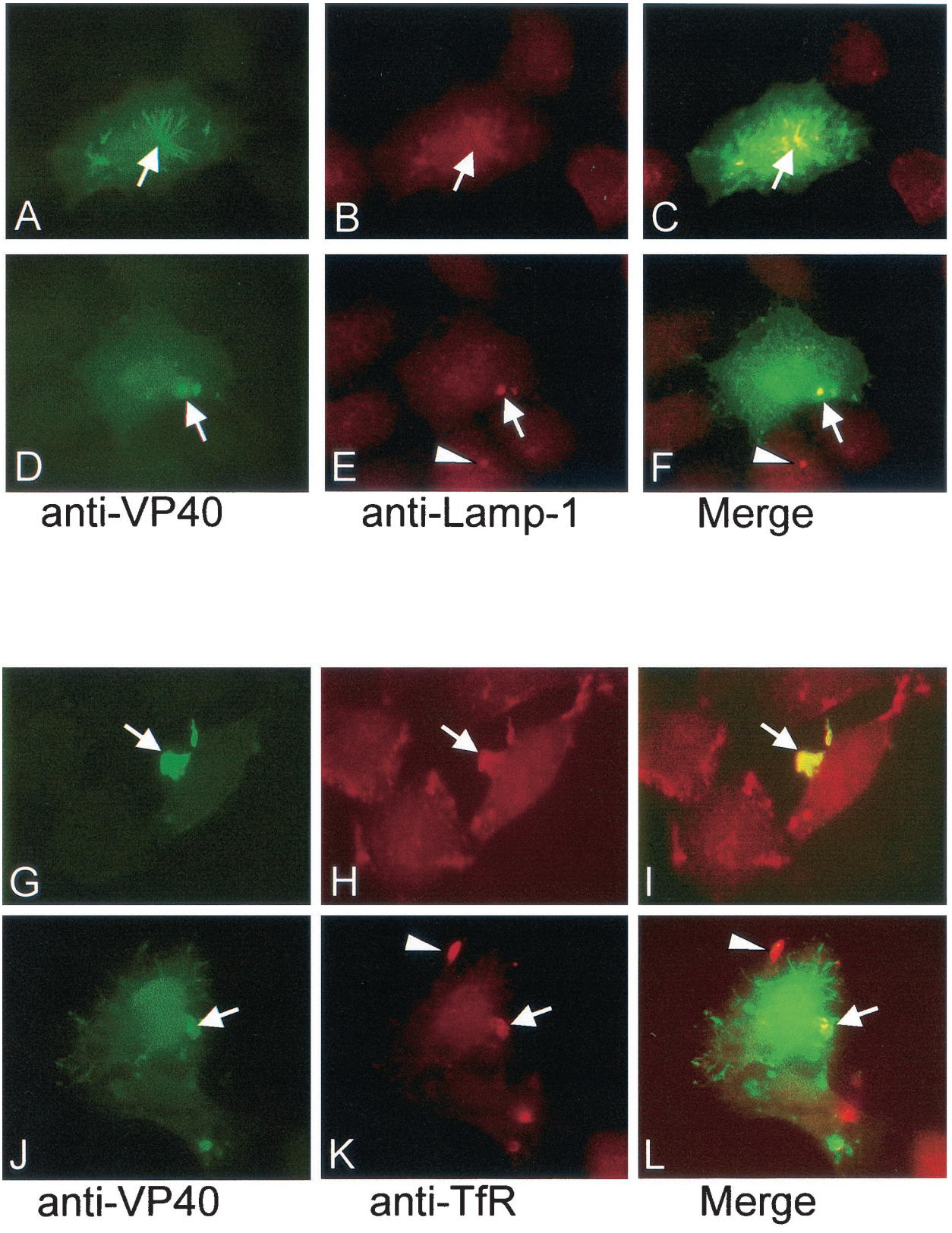

FIG. 5. Immunofluorescence analysis of the intracellular distribution of VP40, Lamp-1, and TfR. HeLa cells were infected with MVA-T7 and transfected with pTM-VP40. At 16 h posttransfection, cells were fixed and immunostained with a rabbit anti-VP40 antibody (dilution, 1:10) and a secondary donkey anti-rabbit IgG conjugated with FITC (dilution, 1:100), together with either an anti-Lamp-1 (A to F) or an anti-TfR (G to L) monoclonal antibody (dilution, 1:20) and a secondary donkey anti-mouse antibody conjugated with rhodamine. (A and D) VP40/FITC. (B and E) Lamp-1–rhodamine. (C and F) Merged images. The arrows indicate the colocalization of VP40 and Lamp-1 in the tubular network (A to C) or in spots (D to F). (E and F) The arrowheads indicate a Lamp-1-positive spot in a VP40-negative cell. (G and J) VP40-FITC. (H and K) TfR-rhodamine. (C and F) Merged images. The arrows indicate sites of overlapping in leading edge of the cell (G to I) or in spots (J to L). (K and L) The arrowheads indicate a TfR-positive leading edge that does not contain VP40.

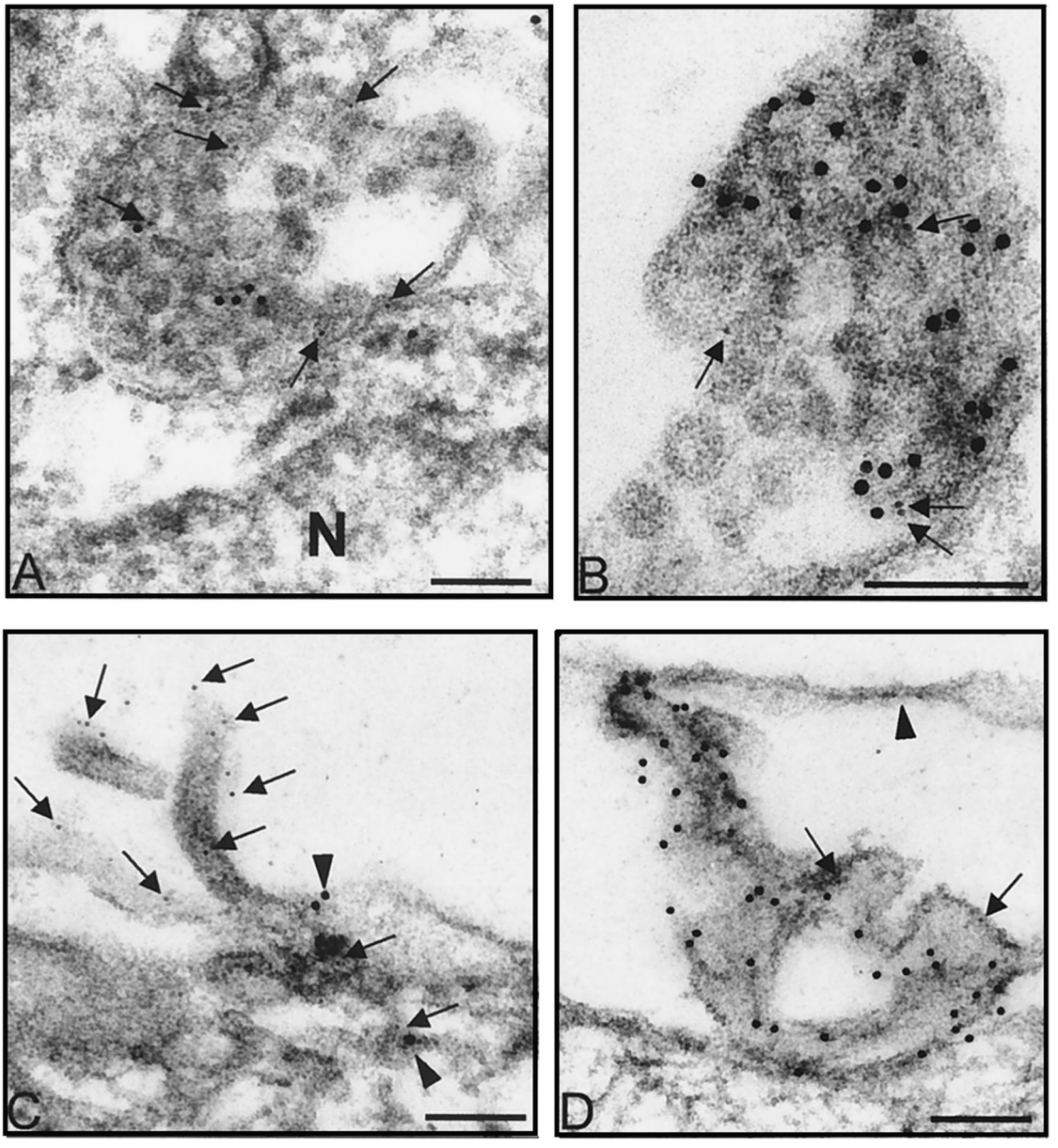

FIG. 6. Immunoelectron microscopic analysis of recombinant VP40 in HeLa cells. HeLa cells were infected with MVA-T7 and transfected with pTM-VP40. At 16 h posttransfection, cells were fixed and immunostained with either a rabbit affinity-purified anti-VP40 antiserum (dilution, 1:10) and an anti-Lamp-1 monoclonal antibody (dilution, 1:20) (A, B, and D) or an anti-VP40 monoclonal antibody (dilution, 1:100) and rabbit IgG against actin (dilution, 1:200) (C). Donkey anti-mouse antibody conjugated with colloidal gold (bead diameter, 6 nm) and donkey anti-rabbit antibody conjugated with colloidal gold (bead diameter, 12 nm) were used as secondary antibodies. (A, B, and D) The arrows indicate Lamp-1 (6-nm gold beads). N, nucleus. In panel D, the arrowhead indicates a site of double membranes. (C) The arrows indicate VP40 (6-nm gold beads), and the arrowheads indicate actin (12-nm gold beads). Bar, 100 nm.

DISCUSSION

VP40 is presumed to represent the matrix protein of MBGV and is therefore believed to be involved in multiple interactions with viral and cellular structures during viral assembly. However, experimental data on the biological features of VP40 have been very restricted. In this study, we analyzed the localization of VP40 in viral particles and inside MBGV-infected cells and characterized recombinantly expressed VP40. We found that VP40, besides the characteristics which are known for matrix proteins of negative-sense RNA viruses, displays a novel feature that is association with the late endosomal compartment.

VP40 is detected in association with nucleocapsid structures and intracellular membranes. In MBGV-infected cells, VP40 was associated with different structures which were divided in two categories. On one hand, VP40 was colocalized with individual nucleocapsids and nucleocapsid-containing structures (viral inclusions). On the other hand, VP40 was found to be

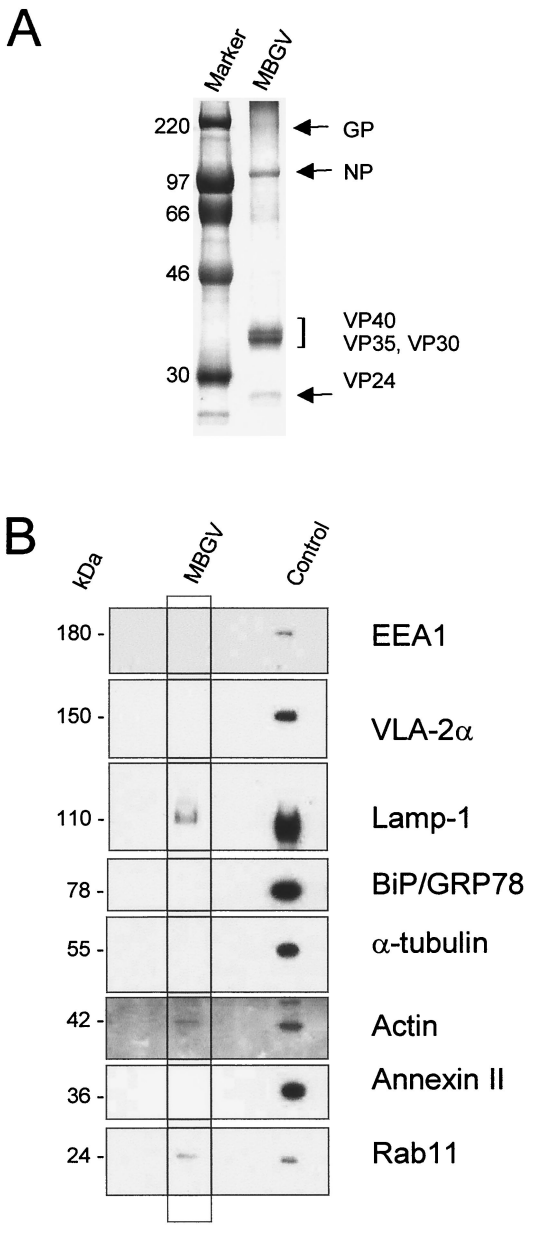

FIG. 7. Western blot analysis of cellular proteins in purified MBGV structural proteins. Purified MBGV structural proteins (20) were separated by SDS-PAGE and either stained with Coomassie blue or blotted onto polyvinylidene difluoride membranes. (A) Coomassie blue staining of purified MBGV structural proteins. (B) Western blot analysis of cellular proteins in purified virions. Mouse monoclonal antibodies directed against marker proteins of early endosomes (EEA1), plasma membrane (VLA-2α), late endosomes (Lamp-1), endoplasmic reticulum (BiP/GRP78), microtubules (α-tubulin), annexin II, and small GTPase (Rab11), or rabbit IgG directed against actin were used to detect the respective proteins. Control, uninfected HeLa cells.

associated with intracellular membrane structures and with the plasma membrane, in foci of plasma membrane proliferation.

The result that VP40 was associated with inclusions, which presumably represent places of nucleocapsid assembly (2, 36), is in line with observations of Geisbert and Jahrling (23), who also detected VP40 inside inclusions. The association of VP40 with single nucleocapsids point to a cotransport of VP40 and nucleocapsids to the sites of virus budding at the plasma membrane.

However, the amount of VP40 in intracellular nucleocapsid structures was seven times less than in mature virions, suggesting that nucleocapsid-associated VP40 does not represent the main source of VP40 in the viral particles.

This presumption was underlined by the finding that various VP40-positive membrane structures were detected, which were free of NP. At first, VP40-containing membrane clusters of a multivesicular or multilayered appearance were identified. Additionally, VP40-positive patches of plasma membrane were detected in the foci of virus-induced membrane proliferation. These findings indicated a nucleocapsid-independent transport of VP40. However, these data did not rule out the possibility that VP40 was recruited to the membranes by the viral surface protein GP or the second putative matrix protein, VP24. Thus, it has been suggested for Sendai virus that the presence of the surface proteins enabled binding of the matrix protein to intracellular membranes (58, 59). To investigate the membrane association capability of VP40 in the absence of other MBGV proteins, we analyzed the distribution of recombinantly expressed VP40.

VP40 is a peripheral membrane protein. Recombinant VP40 displayed a strong association with cellular membranes which was resistant to high salt concentrations, high pH, and treatment with EDTA. These data point to a hydrophobic interaction between VP40 and the membranes which is not dependent on divalent cations. Finally, the Triton X-114 phase-partitioning analysis suggested that VP40 represented a peripheral membrane protein. All of these characteristics are shared by the matrix proteins of other negative-strand RNA viruses, indicating that VP40, indeed, represents the major matrix protein of MBGV (38). Similar findings were published recently for EBOV VP40 which, upon recombinant expression, is also peripherally associated with cellular membranes (33).

VP40-containing membranes have characteristics of the late endosomal compartment. The intracellular VP40-positive membrane clusters both in MBGV-infected and in transiently expressing cells displayed a multivesicular or multilayered structure that was similar to late endosomes (27, 42). Beside the morphologic similarities, the identity of the VP40-positive MVBs is further elucidated by the finding that these membrane structures contained Lamp-1 and the TfR. Both proteins are known to accumulate in MVBs which belong to the late endosomal compartment (30, 41, 51).

Functionally, MVBs have been proposed to act as intermediates on the receptor recycling pathway (42). Recycling of receptors back to the plasma membrane can occur directly from the early endosome (fast cycle) or indirectly via the recycling endosome (31). The transit through the recycling endosome proceeds with slower kinetics than the transport through early endosomes and appears to delay the rate of recycling, causing an accumulation of the intracellular pool of receptors and other plasma membrane components (61, 63). MVBs are also presumed to function as sources of plasma membrane which are necessary for the formation of cellular protrusions during migration and phagocytosis (43). Thus, the forward margins of moving cells contain frequently recycling

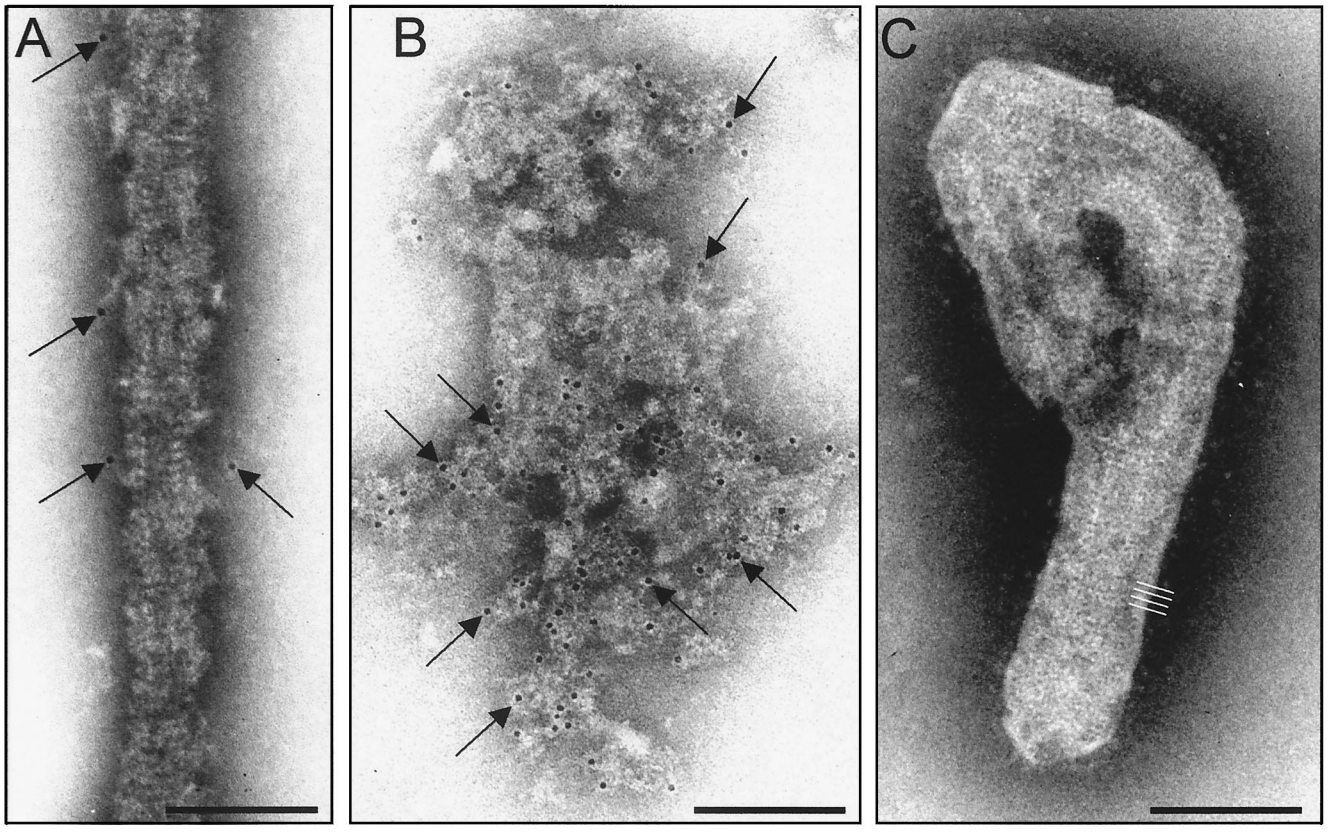

FIG. 8. Immunoelectron microscopic analysis of detergent-treated MBGV particles. Purified virions were treated with Triton X-100 (A and B) or left untreated as a control (C) and immunostained with an anti-VP40 mouse monoclonal antibody and a secondary donkey anti-mouse antibody conjugated with colloidal gold (6-nm gold beads, arrows). White lines indicate regular striation of the viral envelop. Bar, 100 nm.

receptors, even those which are known to reside in recycling endosomes (e.g., the TfR [5, 31, 52]). Additionally, it has been shown that recycling endosomes are associated with cytoskeletal proteins (11, 53) and small GTPases, for example, Rab11 (8, 9, 12, 24, 66).

The high amount of VP40 in MVBs suggests that VP40 can use this intracellular compartment for sorting and accumulation. The mechanisms of this process are not understood. However, the large amounts of unique lipids and an enrichment in lipid rafts found in MVBs (21, 32, 35, 47) may enable specific binding of VP40. It has not yet been observed that matrix proteins of *Mononegavirales* are able to interact with the membranes of late endosomes. However, the M protein of vesicular stomatitis virus, which was expressed by using a recombinant Sendai virus, was bound to membranes, suggested to be derived from intracellular transport vesicles (56). Besides, previous cell fractionation studies have shown that the M protein of Newcastle disease virus (49) and Sendai virus (37) were, indeed, present in the intracellular smooth membrane fraction.

We detected, in addition to its interaction with MVBs, VP40 in association with membranes which formed filopodia- or lamellipodia-like protrusions at the cell surface. These contained Lamp-1, TfR, and actin, suggesting that the intracellular VP40-positive membranes can be transported to the plasma membrane by using the cellular machinery that mediates the transport of recycling endosomes. The detection of traces of proteins specific for late recycling endosomes in mature virions also indicated that the formation of MBGV particles is associated at some stages with the endosomal compartment. The variable intracellular pattern of VP40 distribution appears to be present at different stages of transport of VP40-positive membranes.

In this study we showed for the first time that the matrix protein of MBGV is able to interact with intracellular membranes. The membranes that contained VP40, Lamp-1, and TfR are found intracellularly and as inserted patches in the plasma membrane. These results suggest that VP40 utilizes membranes that display characteristics of the late endosomal compartment for its intracellular transport. The mechanism of formation of VP40-positive membrane clusters, and their association with cytoskeletal proteins, is currently under investigation.

ACKNOWLEDGMENTS

We thank Dagmar Bauer for help with confocal microscopy. We also appreciate the expert technical assistance of Sonja Heck and Angelika Lander.

This work was supported by grants from the Deutsche Forschungsgemeinschaft, Sonderforschungsbereich 286, TP A6, and the Kempkes Stiftung to S.B.

REFERENCES

1. **Becker, S., H.-D. Klenk, and E. Mühlberger.** 1996. Intracellular transport and processing of the Marburg virus surface protein in vertebrate and insect cells. Virology **225:**145–155.
2. **Becker, S., C. Rinne, U. Hofsäss, H.-D. Klenk, and E. Mühlberger.** 1998. Interactions of Marburg virus nucleocapsid proteins. Virology **249:**406–417.
3. **Bergmann, J. E., and P. J. Fusco.** 1988. The M protein of vesicular stomatitis virus associates specifically with the basolateral membranes of polarized epithelial cells independently of the G protein. J. Cell Biol. **107:**1707–1715.
4. **Bordier, C.** 1981. Phase separation of integral membrane proteins in Triton X-114 solution. J. Biol. Chem. **256:**1604–1607.
5. **Bretscher, M. S., and C. Aguado-Velasco.** 1998. Membrane traffic during cell locomotion. Curr. Opin. Cell Biol. **10:**537–541.
6. **Buechi, M., and T. Bachi.** 1982. Microscopy of internal structures of Sendai virus associated with the cytoplasmic surface of host membranes. Virology **120:**349–359.
7. **Bukreyev, A. A., V. E. Volchkov, V. M. Blinov, S. A. Dryga, and S. V. Netesov.** 1995. The complete nucleotide sequence of the Popp (1967) strain of Marburg virus: a comparison with the Musoke (1980) strain. Arch. Virol. **140:** 1589–1600.
8. **Casanova, J. E., X. Wang, R. Kumar, S. G. Bhartur, J. Navarre, J. E. Woodrum, Y. Altschuler, G. S. Ray, and J. R. Goldenring.** 1999. Association of Rab25 and Rab11a with the apical recycling system of polarized Madin-Darby canine kidney cells. Mol. Biol. Cell **10:**47–61.
9. **Chen, W., Y. Feng, D. Chen, and A. Wandinger-Ness.** 1998. Rab11 is required for trans-Golgi network-to-plasma membrane transport and a preferential target for GDP dissociation inhibitor. Mol. Biol. Cell **9:**3241–3257.
10. **Chong, L. D., and J. K. Rose.** 1993. Membrane association of functional vesicular stomatitis virus matrix protein in vivo. J. Virol. **67:**407–414.
11. **Cole, N. B., and J. Lippincott-Schwartz.** 1995. Organization of organelles and membrane traffic by microtubules. Curr. Opin. Cell Biol. **7:**55–64.
12. **Cox, D., D. J. Lee, B. M. Dale, J. Calafat, and S. Greenberg.** 2000. A Rab11-containing rapidly recycling compartment in macrophages that promotes phagocytosis. Proc. Natl. Acad. Sci. USA **97:**680–685.
13. **Elliott, L. H., M. P. Kiley, and J. B. McCormick.** 1985. Descriptive analysis of Ebola virus proteins. Virology **147:**169–176.
14. **Feldmann, H., H. Bugany, F. Mahner, H.-D. Klenk, D. Drenckhahn, and H. J. Schnittler.** 1996. Filovirus-induced endothelial leakage triggered by infected monocytes/macrophages. J. Virol. **70:**2208–2214.
15. **Feldmann, H., E. Mühlberger, A. Randolf, C. Will, M. P. Kiley, A. Sanchez, and H.-D. Klenk.** 1992. Marburg virus, a filovirus: messenger RNAs, gene order, and regulatory elements of the replication cycle. Virus Res. **24:**1–19.
16. **Feldmann, H., C. Will, M. Schikore, W. Slenczka, and H.-D. Klenk.** 1991. Glycosylation and oligomerization of the spike protein of Marburg virus. Virology **182:**353–356.
17. **Felgner, J. H., R. Kumar, C. N. Sridhar, C. J. Wheeler, Y. J. Tsai, R. Border, P. Ramsey, M. Martin, and P. L. Felgner.** 1994. Enhanced gene delivery and mechanism studies with a novel series of cationic lipid formulations. J. Biol. Chem. **269:**2550–2561.
18. **Fujiki, Y., A. L. Hubbard, S. Fowler, and P. B. Lazarow.** 1982. Isolation of intracellular membranes by means of sodium carbonate treatment: application to endoplasmic reticulum. J. Cell Biol. **93:**97–102.
19. **Fujiyoshi, Y., N. P. Kume, K. Sakata, and S. B. Sato.** 1994. Fine structure of influenza A virus observed by electron cryo-microscopy. EMBO J. **13:**318–326.
20. **Funke, C., S. Becker, H. Dartsch, H.-D. Klenk, and E. Mühlberger.** 1995. Acylation of the Marburg virus glycoprotein. Virology **208:**289–297.
21. **Gagescu, R., N. Demaurex, R. G. Parton, W. Hunziker, L. A. Huber, and J. Gruenberg.** 2000. The recycling endosome of Madin-Darby canine kidney cells is a mildly acidic compartment rich in raft components. Mol. Biol. Cell **11:**2775–2791.
22. **Garoff, H., R. Hewson, and D. J. Opstelten.** 1998. Virus maturation by budding. Microbiol. Mol. Biol. Rev. **62:**1171–1190.
23. **Geisbert, T. W., and P. B. Jahrling.** 1995. Differentiation of filoviruses by electron microscopy. Virus Res. **39:**129–150.
24. **Green, E. G., E. Ramm, N. M. Riley, D. J. Spiro, J. R. Goldenring, and M. Wessling-Resnick.** 1997. Rab11 is associated with transferrin-containing recycling compartments in K562 cells. Biochem. Biophys. Res. Commun. **239:** 612–616.
25. **Griffiths, G., R. Back, and M. Marsh.** 1989. A quantitative analysis of the endocytic pathway in baby hamster kidney cells. J. Cell Biol. **109:**2703–2720.
26. **Griffiths, G., and H. Hoppeler.** 1986. Quantitation in immunocytochemistry: correlation of immunogold labeling to absolute number of membrane antigens. J. Histochem. Cytochem. **34:**1389–1398.
27. **Gruenberg, J., and F. R. Maxfield.** 1995. Membrane transport in the endocytic pathway. Curr. Opin. Cell Biol. **7:**552–563.
28. **Harder, T., R. Kellner, R. G. Parton, and J. Gruenberg.** 1997. Specific release of membrane-bound annexin II and cortical cytoskeletal elements by sequestration of membrane cholesterol. Mol. Biol. Cell **8:**533–545.
29. **Harty, R. N., M. E. Brown, G. Wang, J. Huibregtse, and F. P. Hayes.** 2000. A PPxY motif within the VP40 protein of Ebola virus interacts physically and functionally with a ubiquitin ligase: implications for filovirus budding. Proc. Natl. Acad. Sci. USA **97:**13871–13876.
30. **Hopkins, C. R.** 1983. Intracellular routing of transferrin and transferrin receptors in epidermoid carcinoma A431 cells. Cell **35:**321–330.
31. **Hopkins, C. R., A. Gibson, M. Shipman, D. K. Strickland, and I. S. Trowbridge.** 1994. In migrating fibroblasts, recycling receptors are concentrated in narrow tubules in the pericentriolar area, and then routed to the plasma membrane of the leading lamella. J. Cell Biol. **125:**1265–1274.
32. **Hornick, C. A., D. Y. Hui, and J. G. DeLamatre.** 1997. A role for retrosomes in intracellular cholesterol transport from endosomes to the plasma membrane. Am. J. Physiol. **273:**C1075–C1081.
33. **Jasenosky, L. D., G. Neumann, I. Lukashevich, and Y. Kawaoka.** 2001. Ebola virus VP40-induced particle formation and association with the lipid bilayer. J. Virol. **75:**5205–5214.
34. **Kleijmeer, M. J., S. Morkowski, J. M. Griffith, A. Y. Rudensky, and H. J. Geuze.** 1997. Major histocompatibility complex class II compartments in human and mouse B lymphoblasts represent conventional endocytic compartments. J. Cell Biol. **139:**639–649.
35. **Kobayashi, T., F. Gu, and J. Gruenberg.** 1998. Lipids, lipid domains and lipid-protein interactions in endocytic membrane traffic. Semin. Cell Dev. Biol. **9:**517–526.
36. **Kolesnikova, L., E. Muhlberger, E. Ryabchikova, and S. Becker.** 2000. Ultrastructural organization of recombinant Marburg virus nucleoprotein: comparison with Marburg virus inclusions. J. Virol. **74:**3899–3904.
37. **Lamb, R. A., and P. W. Choppin.** 1977. The synthesis of Sendai virus polypeptides in infected cells. II. Intracellular distribution of polypeptides. Virology **81:**371–381.
38. **Lenard, J.** 1996. Negative-strand virus M and retrovirus MA proteins: all in a family? Virology **216:**289–298.
39. **Lodish, H. F., and M. Porter.** 1980. Specific incorporation of host cell surface proteins into budding vesicular stomatitis virus particles. Cell **19:**161–169.
40. **Lotfering, B., E. Mühlberger, T. Tamura, H.-D. Klenk, and S. Becker.** 1999. The nucleoprotein of Marburg virus is target for multiple cellular kinases. Virology **255:**50–62.
41. **Marsh, E. W., P. L. Leopold, N. L. Jones, and F. R. Maxfield.** 1995. Oligomerized transferrin receptors are selectively retained by a lumenal sorting signal in a long-lived endocytic recycling compartment. J. Cell Biol. **129:** 1509–1522.
42. **Mellman, I.** 1996. Endocytosis and molecular sorting. Annu. Rev. Cell Dev. Biol. **12:**575–625.
43. **Mellman, I.** 2000. Quo vadis: polarized membrane recycling in motility and phagocytosis. J. Cell Biol. **149:**529–530.
44. **Modrof, J., C. Möritz, L. Kolesnikova, T. Konakova, B. Hartlieb, A. Randolf, E. Mühlberger, and S. Becker.** 2001. Phosphorylation of Marburg virus VP30 at serines 40 an 42 is critical for its interaction with NP inclusions. Virology **287:**171–182.
45. **Mühlberger, E., B. Lötfering, H.-D. Klenk, and S. Becker.** 1998. Three of the four nucleocapsid proteins of Marburg virus, NP, VP35, and L, are sufficient to mediate replication and transcription of Marburg virus-specific monocistronic minigenomes. J. Virol. **72:**8756–8764.
46. **Mühlberger, E., A. Sanchez, A. Randolf, C. Will, M. P. Kiley, H.-D. Klenk, and H. Feldmann.** 1992. The nucleotide sequence of the L gene of Marburg virus, a filovirus: homologies with paramyxoviruses and rhabdoviruses. Virology **187:**534–547.
47. **Mukherjee, S., T. T. Soe, and F. R. Maxfield.** 1999. Endocytic sorting of lipid analogues differing solely in the chemistry of their hydrophobic tails. J. Cell Biol. **144:**1271–1284.
48. **Murti, K. G., P. S. Brown, W. J. Bean, Jr., and R. G. Webster.** 1992. Composition of the helical internal components of influenza virus as revealed by immunogold labeling/electron microscopy. Virology **186:**294–299.
49. **Nagai, Y., H. Ogura, and H. Klenk.** 1976. Studies on the assembly of the envelope of Newcastle disease virus. Virology **69:**523–538.
50. **Newcomb, W. W., and J. C. Brown.** 1981. Role of the vesicular stomatitis virus matrix protein in maintaining the viral nucleocapsid in the condensed form found in native virions. J. Virol. **39:**295–299.
51. **Oksvold, M. P., E. Skarpen, L. Wierod, R. E. Paulsen, and H. S. Huitfeldt.** 2001. Re-localization of activated EGF receptor and its signal transducers to multivesicular compartments downstream of early endosomes in response to EGF. Eur. J. Cell Biol. **80:**285–294.
52. **Pierini, L. M., M. A. Lawson, R. J. Eddy, B. Hendey, and F. R. Maxfield.** 2000. Oriented endocytic recycling of $\alpha 5\beta 1$ in motile neutrophils. Blood **95:**2471–2480.
53. **Pol, A., D. Ortega, and C. Enrich.** 1997. Identification of cytoskeleton-associated proteins in isolated rat liver endosomes. Biochem. J. **327:**741–746.
54. **Ruigrok, R. W., G. Schoehn, A. Dessen, E. Forest, V. Volchkov, O. Dolnik, H.-D. Klenk, and W. Weissenhorn.** 2000. Structural characterization and membrane binding properties of the matrix protein VP40 of Ebola virus. J. Mol. Biol. **300:**103–112.
55. **Ryabchikova, E. I., L. V. Kolesnikova, and S. V. Netesov.** 1999. Animal pathology of filoviral infections. Curr. Top. Microbiol. Immunol. **235:**145–173.
56. **Sakaguchi, T., T. Uchiyama, Y. Fujii, K. Kiyotani, A. Kato, Y. Nagai, A.**

Kawai, and T. Yoshida. 1999. Double-layered membrane vesicles released from mammalian cells infected with Sendai virus expressing the matrix protein of vesicular stomatitis virus. Virology **263:**230–243.
57. **Sanchez, A., M. P. Kiley, H.-D. Klenk, and H. Feldmann.** 1992. Sequence analysis of the Marburg virus nucleoprotein gene: comparison to Ebola virus and other non-segmented negative-strand RNA viruses. J. Gen. Virol. **73:** 347–357.
58. **Sanderson, C. M., N. L. McQueen, and D. P. Nayak.** 1993. Sendai virus assembly: M protein binds to viral glycoproteins in transit through the secretory pathway. J. Virol. **67:**651–663.
59. **Sanderson, C. M., H. H. Wu, and D. P. Nayak.** 1994. Sendai virus M protein binds independently to either the F or the HN glycoprotein in vivo. J. Virol. **68:**69–76.
60. **Sanger, C., E. Muhlberger, E. Ryabchikova, L. Kolesnikova, H.-D. Klenk, and S. Becker.** 2001. Sorting of Marburg virus surface protein and virus release take place at opposite surfaces of infected polarized epithelial cells. J. Virol. **75:**1274–1283.
61. **Schmid, S. L., R. Fuchs, P. Male, and I. Mellman.** 1988. Two distinct subpopulations of endosomes involved in membrane recycling and transport to lysosomes. Cell **52:**73–83.
62. **Scianimanico, S., G. Schoehn, J. Timmins, R. H. Ruigrok, H.-D. Klenk, and W. Weissenhorn.** 2000. Membrane association induces a conformational change in the Ebola virus matrix protein. EMBO J. **19:**6732–6741.
63. **Sheff, D. R., E. A. Daro, M. Hull, and I. Mellman.** 1999. The receptor recycling pathway contains two distinct populations of early endosomes with different sorting functions. J. Cell Biol. **145:**123–139.
64. **Smith, D. H., B. K. Johnson, M. Isaacson, R. Swanapoel, K. M. Johnson, M. Killey, A. Bagshawe, T. Siongok, and W. K. Keruga.** 1982. Marburg-virus disease in Kenya. Lancet **i:**816–820.
65. **Stricker, R., G. Mottet, and L. Roux.** 1994. The Sendai virus matrix protein appears to be recruited in the cytoplasm by the viral nucleocapsid to function in viral assembly and budding. J. Gen. Virol. **75:**1031–1042.
66. **Ullrich, O., S. Reinsch, S. Urbe, M. Zerial, and R. G. Parton.** 1996. Rab11 regulates recycling through the pericentriolar recycling endosome. J. Cell Biol. **135:**913–924.
67. **van Deurs, B., O. W. Petersen, S. Olsnes, and K. Sandvig.** 1989. The ways of endocytosis. Int. Rev. Cytol. **117:**131–177.
68. **World Health Organization.** 1999. Marburg fever, Democratic Republic of the Congo. Wkly. Epidemiol. Rec. **74:**145.
69. **Weibel, E. R.** 1972. The value of stereology in analysing structure and function of cells and organs. J. Microsc. **95:**3–13.